Published in final edited form as:

J Am Chem Soc. 2018 July 11; 140(27): 8518–8525. doi:10.1021/jacs.8b03691.

Inhibition Mechanisms of Human Indoleamine 2,3 Dioxygenase 1

Ariel Lewis-Ballester[†], **Shay Karkashon**[†], **Dipanwita Batabyal**[‡,§,‖], **Thomas L. Poulos**[‡,§,‖], and **Syun-Ru Yeh**[*,†]

[†]Department of Physiology and Biophysics, Albert Einstein College of Medicine, Bronx, New York 10461, United States

[‡]Department of Molecular Biology and Biochemistry, University of California, Irvine, California 92697, United States

[§]Department of Pharmaceutical Sciences, University of California, Irvine, California 92697, United States

[‖]Department of Chemistry, University of California, Irvine, California 92697, United States

Abstract

Human indoleamine 2,3-dioxygenase 1 (hIDO1) and tryptophan dioxygenase (hTDO) catalyze the same dioxygenation reaction of Trp to generate *N*-formyl kynurenine (NFK). They share high structural similarity, especially in the active site. However, hIDO1 possesses a unique inhibitory substrate binding site (Si) that is absent in hTDO. In addition, in hIDO1, the indoleamine group of the substrate Trp is H-bonded to S167 through a bridging water, while that in hTDO is directly H-bonded to H76. Here we show that Trp binding to the Si site or the mutation of S167 to histidine in hIDO1 retards its turnover activity and that the inhibited activity can be rescued by an effector, 3-indole ethanol (IDE). Kinetic studies reveal that the inhibited activity introduced by Trp binding to the Si site is a result of retarded recombination of the ferryl moiety with Trp epoxide to form NFK and that IDE reverses the effect by preventing Trp from binding to the Si site. In contrast, the abolished activity induced by the S167H mutation is primarily a result of ~5000-fold reduction in the O_2 binding rate constant, possibly due to the blockage of a ligand delivery tunnel, and that IDE binding to the Si site reverses the effect by reopening the tunnel. The data offer new insights into structure-based design of hIDO1-selective inhibitors.

Graphical Abstract

[*]**Corresponding Author** syun-ru.yeh@einstein.yu.edu.

ASSOCIATED CONTENT

Supporting Information

The Supporting Information is available free of charge on the ACS Publications website at DOI: 10.1021/jacs.8b03691.

A table summarizing crystallographic data collection and refinement statistics. Two figures showing the O_2 binding kinetics of the substrate-free wild-type enzyme and electron density maps of the Trp and/or IDE bound in the S167H mutant (PDF)

Notes

The authors declare no competing financial interest.

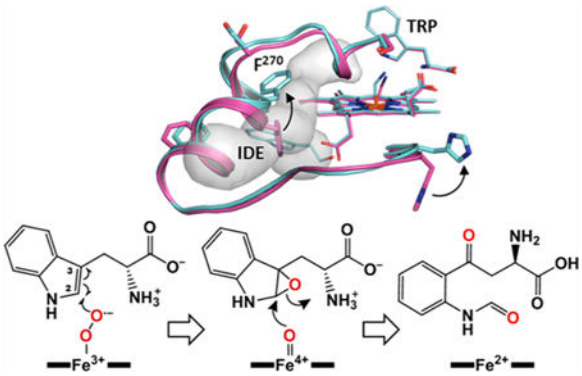

INTRODUCTION

L-Tryptophan (Trp) is the least abundant essential amino acid. The majority of dietary Trp (~95%) is metabolized to nicotinamide adenine dinucleotide (NAD) via the kynurenine (KYN) pathway.[1,2] The first and rate-limiting step of the KYN pathway, the dioxygenation of Trp to *N*-formylkynurenine (NFK), is catalyzed by human indoleamine 2,3-dioxygenase 1 (hIDO1) and tryptophan dioxygenase (hTDO). In addition, to control Trp flux along the KYN pathway, hIDO1 and hTDO are involved in cancer immune escape via the Trp → KYN → AhR pathway.[3–7] Consequently, they have been considered as two important drug targets for cancer immunotherapy.[8–12] While the roles of hIDO1 and hTDO in cancer biology have been subject to extensive studies, molecular properties of the two enzymes remain elusive.

hIDO1 and hTDO belong to one of the three major classes of heme-based enzymes that utilize atmospheric O_2 as a substrate.[13] Oxidases, such as cytochrome *c* oxidase, reduce O_2 to two water molecules by utilizing four electrons and four protons and harness the redox energy to pump four protons across the protein matrix. Monooxygenases, such as P450, convert one atom of dioxygen to a water by consuming two electrons and two protons and exploit the redox energy to insert the other oxygen atom into an organic substrate. Dioxygenases, including hIDO1 or hTDO, are unique as they insert both atoms of O_2 into Trp without utilizing the free energy derived from any oxygen reduction reaction.

Previous spectroscopic studies, combined with QM/MM simulations, suggest that the Trp dioxygenation reactions catalyzed by hIDO1 and hTDO follow the same two-step ferryl-based mechanism (Scheme 1A).[14–16] The reaction is initiated by O_2 and Trp binding to the deoxy enzyme to form the active ternary complex, with a ferric superoxide electronic configuration. The iron-bound dioxygen is then inserted into the C_2 of the Trp through a radical addition reaction to generate the ferryl and Trp-epoxide intermediate (via an alkylperoxo transition state). The ferryl moiety then recombines with Trp-epoxide to form the product NFK. As the ferryl species is relatively inert, the recombination reaction presumably relies on its favorable regioorientation with respect to the Trp-epoxide.

Although hIDO1 and hTDO follow the same two-step ferryl-based mechanism, the multiple turnover activity of hIDO1, but not hTDO, is subject to substrate inhibition.[17] A two-Trp

binding sites model (Scheme 1B) proposed by Lu et al. suggests that at low [Trp] (< ~40 μM), the substrate binds to the active site (Sa) to generate the active ternary complex, which turns over to make NFK; while, at high [Trp], a second Trp can occupy a hypothesized inhibitory site (Si) to generate a two-Trp bound inhibitory complex with compromised activity.

The threshold for substrate inhibition in hIDO1 lies in the normal plasma Trp level (~50–100 μM),[18] suggesting that it is probably important for maintaining a steady synthesis of KYN pathway metabolites, whose overproduction can be hazardous to cells, in particular when large [Trp] fluctuations arise during meals. This type of substrate-controlled regulation is perhaps not required for hTDO as it is a constitutive enzyme, whose activity is constantly regulated at the protein level through an ubiquitination-linked proteasome degradation pathway.[19]

As hIDO1 and hTDO exhibit very low direct sequence homology, they were originally considered as two unrelated enzymes. However, structural studies surprisingly revealed that they share high structural similarity, in particular in the Sa site located in the distal heme pocket.[19–21] More recent structural studies confirm the presence of the inhibitory substrate binding site, Si, on the proximal side of the heme in hIDO1,[21] but not in hTDO.[19] It was documented that, other than Trp, the Si site can bind an effector, 3-indole ethanol (IDE).[17,21] IDE, unlike Trp, preferentially binds to the Si site (Scheme 1C);[21] in addition, the occupation of the Si site by IDE promotes, rather than retards, the enzyme activity. While the reported data clearly demonstrated that hIDO1 activity can be tuned by modulating the structure of the small molecule occupying the Si site, the molecular mechanism remains unclear.

In addition to the Si site, hIDO1 exhibits several unique structural features distinguishing it from hTDO.[19,21] Most notably, in hIDO1, S167 forms water-mediated H-bonds with the indoleamine group of the substrate Trp bound in the Sa site; while in hTDO, S167 is replaced by H76, which forms a direct H-bond with the indoleamine group of the Trp (Scheme 1C–D). Biochemical studies show that the S167H mutation in hIDO1[22] or the H76S mutation in hTDO[23] dramatically reduces the turnover activity of each enzyme.

In this work, we sought to use spectroscopic and crystallographic methods to interrogate the molecular mechanisms by which the occupation of the Si site by Trp or IDE and/or the S167H mutation in hIDO1 perturbs the enzyme activity.

RESULTS

Substrate Inhibition Is a Result of Impeded Recombination of the Ferryl Moiety with the Trp-Epoxide.

The apparent K_d (Trp) of the Sa and Si sites determined during enzyme turnover are 23 and 70 μM, respectively.[21] Spectroscopic studies showed that the two K_d values are sensitive to the oxidation and coordination states of the heme iron.[24,24] In any case, the Sa site, in general, exhibits a much higher Trp affinity than the Si site. To interrogate how the occupation of the Si site by Trp retards enzyme activity, we examined the hIDO1 reaction in

the presence of 40 μM (under which the Sa site is mostly saturated by Trp, while the Si site is minimally occupied), versus 10 mM Trp (under which both the Sa and Si sites are saturated by Trp).[21]

In the presence of 40 μM Trp, the reaction is initiated by O_2 and Trp binding to the deoxy enzyme (λ_{max} = 426/556 nm) to form the active ternary complex (λ_{max} = 413/544/578 nm) (Figure 1A). The apparent k_{on}, 60 s^{-1}, is similar to that observed in the absence of the substrate (Figure S1), indicating that under the condition employed, O_2 binding precedes Trp binding (as a previous study revealed that Trp binding significantly retards O_2 binding),[26] and that the observed k_{on} reflects the O_2 binding rate constant. The fact that the substrate-free oxy complex (λ_{max} = 415/542/576 nm, see Figure S1) was not detected during the reaction indicates that O_2 binding facilitates Trp binding.

Once the ternary complex is completely formed, its concentration remains almost constant up to ~1 s (Figure 1B), as indicated by the kinetic trace at 415 nm shown in the inset. The constant population of the ternary complex leads to active turnover, with an apparent product formation rate constant (k_{NFK}) of 2.1 s^{-1} (calculated based on the kinetic trace at 321 nm). As the substrate Trp is slowly consumed, the ternary complex gradually converts to the substrate-free oxy complex, as suggested by the progressive shift of the Soret maximum from 413 to 415 nm. In a much longer time window (Figure 1C), the substrate-free oxy complex autooxidizes to its ferric form (presumably by releasing superoxide), as indicated by the shift of the Soret maximum from 415 to 406 nm.

The observation that during active turnover (i.e., Step (2) in Figure 1B) only the active ternary complex is populated indicates that (i) O_2 and Trp binding occurs much faster than the dioxygenase chemistry (hence the deoxy complex is not detected), and (ii) the recombination of the ferryl and Trp-epoxide to form NFK occurs much faster than its formation from the active ternary complex (hence the ferryl and Trp-epoxide intermediate, [Fe^{4+}=O W^o], is not detected).

The comparable reaction observed in the presence of 10 mM Trp is also initiated by O_2 and Trp binding to the deoxy enzyme to form the ternary complex (λ_{max} = 415/547/576 nm) (Figure 2A). However, the apparent k_{on} is ~4-fold slower (14 s^{-1}), indicating that Trp is pre-bound to the enzyme prior to O_2 binding, and that Trp binding retards O_2 binding, as reported previously.[24,26]

The ternary complex then constantly turns over to make NFK (Figure 2B). At the same time, a shoulder at 591 nm, characteristic for the ferryl derivative of hIDO1,[14,24,27] is slowly developed. We postulate that during turnover the ternary complex can leak out of the reactive cycle to form the [Fe^{4+}=O W^o]$_W$ species (where the subscripted "W" indicates the occupation of the Si site by Trp). The leakage of the active ternary complex to form the [Fe^{4+}=O W^O]$_W$ species leads to a ~ 2-fold slower apparent k_{NFK} (0.9 s^{-1}). The [Fe^{4+}=O W^o]$_W$ species persists up to ~1000 s (Figure 2C), during which a minute amount of NFK is produced. In a much longer time window, the enzyme slowly converts to the resting ferric state (data not shown), probably due to an autoxidation process.

Taken together the data suggest that Trp binding to the Si site introduces conformational changes to the Sa site, which perturbs the regioorientation of the ferryl with respect to the Trp-epoxide, thereby retarding their recombination to generate NFK.

IDE Promotes Enzyme Turnover by Preventing Trp from Binding to the Si Site.

To investigate the effect of IDE, we carried out side-by-side comparison of the hIDO1 reaction in the absence versus presence of IDE. Here 150 μM Trp and 2 mM IDE were employed to ensure that [Trp] is high enough to saturate the Si site, yet low enough to allow IDE to replace it.[21] The reactions were conducted at 10 °C, so that they can be compared with the S167H reaction (*vide infra*).

In the absence of IDE, the progression of the reaction (Figure 3A–C) is similar to that shown in Figure 2. The presence of 2 mM IDE reduces the apparent k_{on} from 31 to 17 s^{-1} (Figure 3D). The k_{on} is sensitive to [O_2] (data not shown), indicating that it reflects the O_2 binding rate constant. The population of the [Fe^{4+}=O W^{O}]$_W$ species is significantly reduced (as indicated by its spectral marker at 594 nm in Figure 3B vs 3E). In a longer time window, the oxy complex gradually converts to the inactive ferric species, with an apparent k_{ox} of 0.07 s^{-1} (Figure 3F).

The data indicate that the occupation of the Si site by IDE (Scheme 1C), unlike Trp, does not introduce adverse structural changes to the Sa site, and that IDE rescues the enzyme activity by blocking the Si site from Trp binding.

S167H Mutation Severely Retards O_2 Binding That Can Be Rescued by IDE Binding to the Si Site.

To evaluate the effect of S167H mutation, we first examined its turnover activity. As shown in Figure 4A, the mutation almost totally abolishes the enzyme activity as reported preiously.[22] Surprisingly, it can be dramatically rescued by IDE, leading to an apparent K_m of 20 μM and a k_{cat} of 0.6 s^{-1}.

IDE titration studies show that, at low [IDE], it promotes enzyme activity with an apparent K_d of 200 μM (see the inset), likely due to its binding to the Si site, as that observed in the wild-type enzyme.[21] At relatively high [IDE], an increase in [IDE] leads to a decrease in the activity, with an apparent K_d of 500 μM, suggesting that IDE can act as a competitive inhibitor by competing with Trp for the Sa site. Comparable IDE titration of the wild-type enzyme shows a similar K_d toward the Si site (230 μM), but a much higher K_d toward the Sa site ($\gg$10 mM).[21]

We next examined the reaction kinetics of the S167H mutant. The mixing of the ferrous deoxy enzyme (λ_{max} = 432/ 558 nm) with Trp and O_2 unexpectedly leads to an inactive ferric species (λ_{max} = 409/500/631 nm), without populating any active ternary complex, while the addition of IDE dramatically stabilizes the ternary complex (λ_{max} = 417/544/578 nm) (see the red trace in Figure 4C). The data suggest that the abolished activity of the S167H mutant is a result of facilitated autoxidation of the ternary complex and/or retarded O_2/Trp binding to form the ternary complex and that IDE rescues the activity by stabilizing the ternary complex.

To further delineate the mechanism by which S167H mutation abolishes the enzyme activity and that by which IDE rescues it, we examined the mutant reaction under the condition comparable to that employed for the wild-type reaction (Figure 3), with an exception that an O_2-staturated buffer ($[O_2] \sim 1.25$ mM), instead of an air-saturated buffer ($[O_2] \sim 0.25$ mM), was used to facilitate the O_2 binding reaction. This distinct condition leads to partial accumulation of the active ternary complex as well as the inactive $[Fe^{4+}{=}O\ W^{O}]_W$ species (as indicated by the appearance of the 594 nm band), before the enzyme is fully oxidized to the ferric species (Figure 5A–C).

The progression of the reaction is in general similar to that observed in the wild-type reaction (Figure 3). The kinetics, however, is significantly perturbed. Like that observed in the wild-type reaction, the apparent k_{on} for O_2 and Trp binding to the deoxy species to form the ternary complex, 0.03 s^{-1}, is sensitive to $[O_2]$ (data not shown), indicating that the reaction is rate limited by O_2 binding and that the rate constant reflects the O_2 binding rate constant. The bimolecular O_2 binding rate constant, 48 M^{-1} s^{-1} (calculated based on $[O_2]$ = 625 μM), is ~5000-fold lower than that of the comparable wild-type reaction (2.5×10^5 M^{-1} s^{-1}, calculated based on $[O_2]$ = 125 μM). In addition, the apparent k_{NFK} is reduced by ~30-fold.

In the presence of IDE (Figure 5D–E), the inactive $[Fe^{4+}{=}O\ W^{o}]_W$ species is no longer detected (as indicated by the disappearance of the 594 nm band), consistent with the view that IDE competes with Trp for the Si site. Remarkably, the bimolecular O_2 binding rate constant is increased by ~800-fold (from 48 to 4.0×10^4 M^{-1} s^{-1}). As a result, the apparent k_{NFK} is 3-fold faster, despite the fact that the apparent k_{ox} is significantly elevated. These data indicate that the abolished activity of the S167H mutant is mostly a result of the impeded O_2 binding reaction and that IDE rescues the activity by promoting O_2 binding, presumably via binding to the Si site.

S167H Mutation Blocks a Ligand Delivery Tunnel That Is Reopened by IDE Binding to the Si Site.

We then crystallized the S167H-CN-Trp complex in the absence or presence of IDE and refined its structure to a resolution of 2.5 and 2.6 Å, respectively (Table S1).

The replacement of S167 with a histidine in the mutant allows its side chain to form a direct H-bond with the indoleamine group of the Trp (see the upper left inset in Figure 6A), in a fashion similar to that found in hTDO.[19] The larger size of the new side chain pushes the indole ring of the Trp away from it by ~0.6 Å. As a result, the distance between the terminal N atom of the CN ligand and the C_2 of the Trp is slightly longer (Figure 6B).

The mutation does not perturb the overall structure of the enzyme (Figure 6A), however, it significantly modulates the heme binding pocket, in particular in the region near DE-Loop, E-Helix, and EF-Loop (highlighted in magenta in Figure 6A), where the backbone conformations are significantly perturbed; in addition, the side chains of F270 and H287 undergo large-scale rotations (Figure 6B). Intriguingly, these structural changes are localized in a region that coincides with a previously identified water tunnel.[21] The tunnel enters from the corner connecting E-Helix to EF-Loop and runs along E-Helix to the region near F270,

where it bifurcates into two branches. One branch extends into the Sa site along the DE-Loop, while the other branch reaches out to the Si site on the proximal side of the heme. The downward movement of the F270 side chain induced by the mutant partially blocks the water tunnel.

In the presence of IDE, IDE is identified in the Si site (Figure 6C) with a binding pose similar to that observed in the wild-type complex.[21] The occupation of the Si site by IDE surprisingly reverses the mutant structure back to a wild-type like conformation. In particular, it moves the F270 side chain up, which presumably reopens the water tunnel.

Taken together the kinetic and crystallographic data suggest that the water tunnel is a conduit that delivers O_2 into the Sa site during enzyme turnover, that the severely retarded O_2 binding kinetics of the S167H mutant is a result of the clogged ligand delivery tunnel, and that IDE rescues the activity by reopening the tunnel.

CONCLUDING REMARKS

The work presented here reveals that the occupation of the Si site by Trp in the wild-type hIDO1 elicits the inhibition effect by impeding the recombination of the ferryl with Trp-epoxide, without significantly perturbing the initial O_2 binding and insertion or the subsequent O−O bond cleavage. It also underscores the importance of the water tunnel in delivering O_2 into the Sa site during active enzyme turnover. The fact that the Si site and water tunnel are unique to hIDO1 suggests that they present novel target sites for structure-based design of new generations of hIDO1-selective inhibitors.

EXPERIMENTAL SECTION

Protein Expression and Purification.

The S167H mutant was constructed with QuikChange II Site-Directed Mutagenesis Kit (Stratagene, La Jolla, CA) and verified by DNA sequencing. The mutant protein was expressed and purified following the same protocol as that for the wild-type protein.[17,28,29] The purified proteins were stored in pH 7.4 Tris buffer (50 mM) at −80 °C until usage.

Stopped-Flow Measurements.

The experiments were performed by 1:1 mixing of the deoxy ferrous enzymes with a Trp-containing air-saturated buffer (~0.25 mM O_2)[30] or O_2-saturated buffer (~1.25 mM O_2)[30] in a π^* 180 system from Applied Photophysics Ltd. (Leatherhead, Surrey, UK). The deoxy ferrous enzyme was prepared by stoichiometrically titrating N_2-purged ferric enzyme with dithionite; a minute excess dithionite was added to ensure the system was fully anaerobic before mixing. All the solutions were prepared in pH 7.4 Tris buffer (50 mM). The experiments were carried out with the temperature controlled at 20 or 10 °C by a circulating water bath (Neslab RTE-9DD).

Activity Measurements.

The steady-state activities were measured with 0.25 μM enzyme in 50 mM Tris buffer (pH 7.4) at 25 °C with a standard protocol.[17,28,29] The initial linear velocities of the reactions, v,

were obtained by monitoring the formation of the product, NFK, at 321 nm (ε = 3750 $M^{-1}cm^{-1}$) as a function of time with a UV2100 spectrophotometer (Shimadzu Scientific Instruments, Inc.) with a spectral slit width of 2 nm. The v was calibrated with the concentration of the enzyme. The IDE titration was carried out with 0.1 mM Trp. All the data were analyzed with Origin 6.1 software (Microcal Software, Inc., MA).

Crystal Preparation.

The growth of S167H-CN-Trp complex crystal was initiated by mixing a protein solution (40 mg/mL) with a precipitant solution (100 mM sodium thiosulfate in 100 mM CAPS buffer (pH 10.0) and 20% (w/v) PEG 8000). Crystals were grown at 4 °C using the microbatch method. The S167H-CN-Trp complex was prepared with 10 mM Trp in the absence of IDE or 2 mM Trp in the presence of 10 mM IDE. The crystal was cryoprotected by supplementing the mother solution with 20% (v/v) ethylene glycol before it was flash-frozen in liquid nitrogen for data collection.

Crystallographic Data Collection and Analysis.

The data were collected remotely using the Stanford Synchrotron Radiation Lightsource (SSRL) beamline 9–2. The diffraction images were indexed, integrated, and scaled with XDS[31] and Aimless.[32] The Karplus–Diederichs method[33] was used to find a proper resolution cutoff for each structure. Molecular replacement was conducted with Phaser[35] through the CCP4i graphic interface[35] using the 4-phenylimidazole complex structure (PDB code: 2D0T) as the search model. Further model building was performed using COOT.[36] Structure refinements were performed using Refmac5.[35,37,38] Data processing and refinement statistics are summarized in Table S1. The structural models were displayed with PyMOL (http://www.pymol.org/), based on the subunit B, as its electron density is stronger than that of the subunit A. The PDB codes of the S167H-CN-Trp complexes without and with IDE are 6CXU and 6CXV, respectively. The electron density maps of Trp and IDE are shown in Figure S2.

Supplementary Material

Refer to Web version on PubMed Central for supplementary material.

ACKNOWLEDGMENTS

We thank Dr. Denis L. Rousseau for helpful discussions. The structural data were collected at Stanford Synchrotron Radiation Lightsource, a national user facility operated by Stanford University on behalf of the United States Department of Energy, Office of Basic Energy Sciences. The Stanford Synchrotron Radiation Lightsource Structural Molecular Biology Program is supported by the United States Department of Energy, Office of Biological and Environmental Research and by the National Center for Research Resources, Biomedical Technology Program, and NIGMS of the National Institutes of Health. We acknowledge the contributions from Drs F. Forouhar, S. Lew, J. Seetharaman, and L. Tong to the initial stage of this project. This work was supported by National Institute of Health Grant GM115773 and National Science Foundation Grant CHE-1404929 (to S.-R.Y.) and National Institute of Health Grant GM57353 (to T.L.P.).

REFERENCES

(1). Leklem JE Am. J. Clin. Nutr 1971, 24 (6), 659–72. [PubMed: 4253043]

(2). Takikawa O Biochem. Biophys. Res. Commun 2005, 338 (1), 12–9. [PubMed: 16176799]

(3). Uyttenhove C; Pilotte L; Theate I; Stroobant V; Colau D; Parmentier N; Boon T; Van den Eynde BJ Nat. Med 2003, 9 (10), 1269–74. [PubMed: 14502282]

(4). Pilotte L; Larrieu P; Stroobant V; Colau D; Dolusic E; Frederick R; De Plaen E; Uyttenhove C; Wouters J; Masereel B; Van den Eynde BJ Proc. Natl. Acad. Sci. U. S. A 2012, 109 (7), 2497–502. [PubMed: 22308364]

(5). Muller AJ; DuHadaway JB; Donover PS; Sutanto-Ward E; Prendergast GC Nat. Med 2005, 11 (3), 312–9. [PubMed: 15711557]

(6). Bessede A; Gargaro M; Pallotta MT; Matino D; Servillo G; Brunacci C; Bicciato S; Mazza EM; Macchiarulo A; Vacca C; Iannitti R; Tissi L; Volpi C; Belladonna ML; Orabona C; Bianchi R; Lanz TV; Platten M; Della Fazia MA; Piobbico D; Zelante T; Funakoshi H; Nakamura T; Gilot D; Denison MS; Guillemin GJ; DuHadaway JB; Prendergast GC; Metz R; Geffard M; Boon L; Pirro M; Iorio A; Veyret B; Romani L; Grohmann U; Fallarino F; Puccetti P Nature 2014, 511 (7508), 184–90. [PubMed: 24930766]

(7). Mellor AL; Munn DH Nat. Rev. Immunol 2004, 4 (10), 762–74. [PubMed: 15459668]

(8). Mullard A Nat. Rev. Drug Discovery 2015, 14, 373.

(9). Sheridan C Nat. Biotechnol 2015, 33 (4), 321–2. [PubMed: 25850038]

(10). Huggett B Nat. Biotechnol 2015, 33, 470–7. [PubMed: 25965753]

(11). Prendergast GC; Malachowski WP; DuHadaway JB; Muller AJ Cancer Res 2017, 77 (24), 6795–6811. [PubMed: 29247038]

(12). Rohrig UF; Majjigapu SR; Vogel P; Zoete V; Michielin OJ Med. Chem 2015, 58 (24), 9421–37.

(13). Sono M; Roach MP; Coulter ED; Dawson JH Chem. Rev 1996, 96 (7), 2841–2888. [PubMed: 11848843]

(14). Lewis-Ballester A; Batabyal D; Egawa T; Lu C; Lin Y; Marti MA; Capece L; Estrin DA; Yeh SR Proc. Natl. Acad. Sci. U. S. A 2009, 106 (41), 17371–6. [PubMed: 19805032]

(15). Capece L; Lewis-Ballester A; Batabyal D; Di Russo N; Yeh SR; Estrin DA; Marti MA JBIC, J. Biol. Inorg. Chem 2010, 15 (6), 811–23. [PubMed: 20361220]

(16). Capece L; Lewis-Ballester A; Yeh SR; Estrin DA; Marti MA J. Phys. Chem. B 2012, 116 (4), 1401–13. [PubMed: 22196056]

(17). Lu C; Lin Y; Yeh SR J. Am. Chem. Soc 2009, 131 (36), 12866–7. [PubMed: 19737010]

(18). Torres MI; Lopez-Casado MA; Lorite P; Rios A Clin. Exp. Immunol 2007, 148 (3), 419–24. [PubMed: 17362267]

(19). Lewis-Ballester A; Forouhar F; Kim SM; Lew S; Wang Y; Karkashon S; Seetharaman J; Batabyal D; Chiang BY; Hussain M; Correia MA; Yeh SR; Tong L Sci. Rep 2016, 6, 35169. [PubMed: 27762317]

(20). Sugimoto H; Oda S; Otsuki T; Hino T; Yoshida T; Shiro Y Proc. Natl. Acad. Sci. U. S. A 2006, 103 (8), 2611–6. [PubMed: 16477023]

(21). Lewis-Ballester A; Pham KN; Batabyal D; Karkashon S; Bonanno JB; Poulos TL; Yeh SR Nat. Commun 2017, 8 (1), 1693. [PubMed: 29167421]

(22). Chauhan N; Basran J; Efimov I; Svistunenko DA; Seward HE; Moody PC; Raven EL Biochemistry 2008, 47 (16), 4761–9. [PubMed: 18370410]

(23). Batabyal D; Yeh SR J. Am. Chem. Soc 2009, 131 (9), 3260–70. [PubMed: 19209904]

(24). Lu C; Lin Y; Yeh SR Biochemistry 2010, 49 (24), 5028–34. [PubMed: 20476772]

(25). Lu C; Yeh SR J. Biol. Chem 2011, 286 (24), 21220–30. [PubMed: 21502325]

(26). Efimov I; Basran J; Sun X; Chauhan N; Chapman SK; Mowat CG; Raven EL J. Am. Chem. Soc 2012, 134 (6), 3034–41. [PubMed: 22299628]

(27). Yanagisawa S; Yotsuya K; Hashiwaki Y; Horitani M; Sugimoto H; Shiro Y; Appelman EH; Ogura T Chem. Lett 2010, 39 (1), 36–37.

(28). Shimizu T; Nomiyama S; Hirata F; Hayaishi OJ Biol. Chem 1978, 253 (13), 4700–4706.

(29). Sono M; Taniguchi T; Watanabe Y; Hayaishi OJ Biol. Chem 1980, 255 (4), 1339–1345.

(30). Coin JT; Olson JS J. Biol. Chem 1979, 254 (4), 1178–1190. [PubMed: 762123]

(31). Otwinowski Z; Minor W Methods Enzymol 1997, 276, 307–26.

(32). Evans PR; Murshudov GN Acta Crystallogr., Sect. D: Biol. Crystallogr 2013, 69 (7), 1204–1214. [PubMed: 23793146]

(33). Karplus PA; Diederichs K Science 2012, 336 (6084), 1030–3. [PubMed: 22628654]

(34). McCoy AJ; Grosse-Kunstleve RW; Adams PD; Winn MD; Storoni LC; Read RJ J. Appl. Crystallogr 2007, 40 (4), 658–674. [PubMed: 19461840]

(35). Winn MD; Ballard CC; Cowtan KD; Dodson EJ; Emsley P; Evans PR; Keegan RM; Krissinel EB; Leslie AG; McCoy A; McNicholas SJ; Murshudov GN; Pannu NS; Potterton EA; Powell HR; Read RJ; Vagin A; Wilson KS Acta Crystallogr., Sect. D: Biol. Crystallogr 2011, 67 (4), 235–42. [PubMed: 21460441]

(36). Emsley P; Cowtan K Acta Crystallogr., Sect. D: Biol. Crystallogr 2004, 60 (12), 2126–2132. [PubMed: 15572765]

(37). Murshudov GN; Skubak P; Lebedev AA; Pannu NS; Steiner RA; Nicholls RA; Winn MD; Long F; Vagin AA Acta Crystallogr., Sect. D: Biol. Crystallogr 2011, 67 (4), 355–367. [PubMed: 21460454]

(38). Murshudov GN; Vagin AA; Dodson EJ Acta Crystallogr., Sect. D: Biol. Crystallogr 1997, 53 (3), 240–255. [PubMed: 15299926]

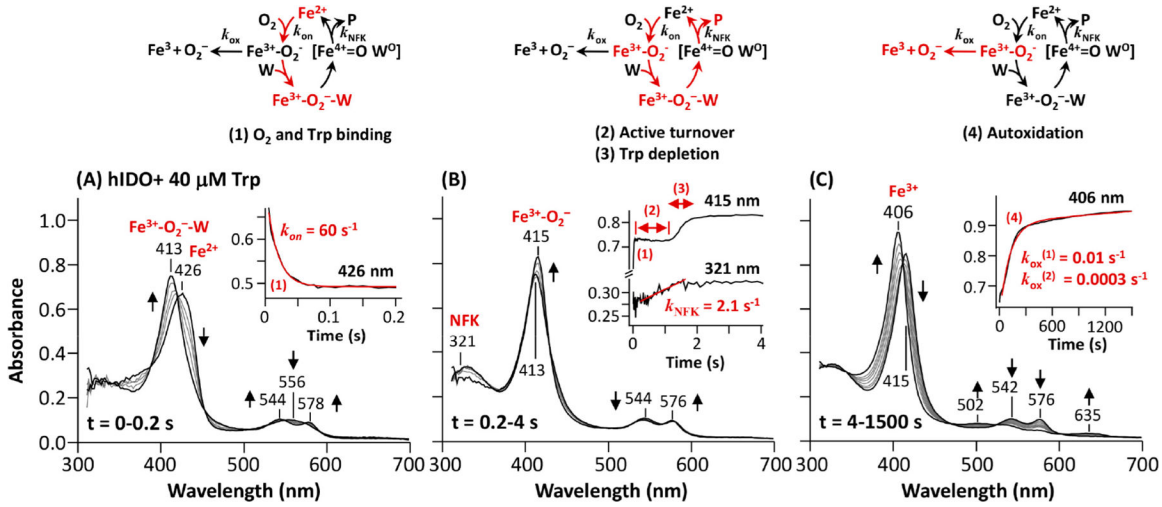

Figure 1. Reaction kinetics of hIDO1 in the presence of 40 μM Trp.

The spectra were obtained as a function of time following the initiation of the reaction by mixing an air-saturated buffer with ferrous deoxy hIDO1 (in the presence of Trp) in a stopped-flow system at 20 °C. The final [hIDO1], [O_2] and [Trp] were 6, 125, and 40 μM, respectively, after mixing. The time window associated with the spectral data shown in each panel is indicated in the lower left corner. In each panel, the progression of the reaction is highlighted in the kinetic trace(s) shown in the inset, where the key kinetic constants are indicated. A schematic illustration of the reaction cycle is shown at the top of each panel, where the elementary steps of the reaction occurring within the given time window, as well as the detectable intermediates, are highlighted in red. "W" stands for Trp, while [Fe^{4+}=O W^{o}] stands for the hypothesized ferryl and Trp-epoxide intermediate.

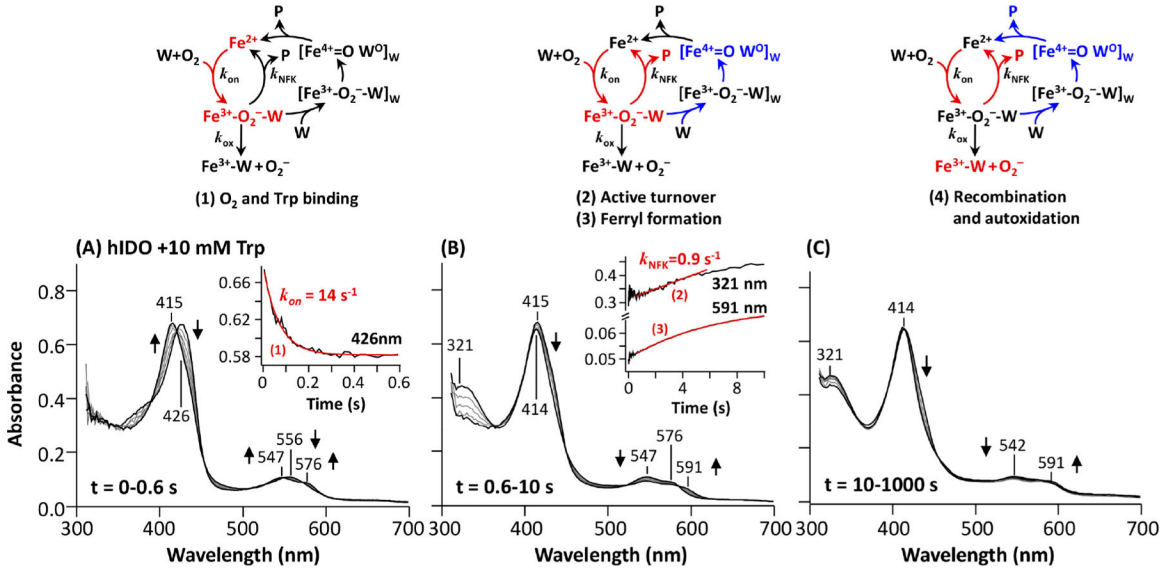

Figure 2. Reaction kinetics of hIDO1 in the presence of 10 mM Trp.

The spectra were obtained as a function of time following the initiation of the reaction by mixing an air-saturated buffer with ferrous deoxy hIDO1 (in the presence of Trp) in a stopped-flow system at 20 °C. The final [hIDO1], [O_2] and [Trp] were 6 μM, 125 μM and 10 mM, respectively, after mixing. The time window associated with the spectral data shown in each panel is indicated in the lower left corner. In each panel, the progression of the reaction is highlighted in the kinetic trace(s) shown in the inset, where the key kinetic constants are indicated. A schematic illustration of the reaction cycle is shown at the top of each panel, where the elementary steps of the reaction occurring within the given time window, as well as the detectable intermediates, are highlighted in red and blue. The hypothesized intermediate, [Fe^{4+}=O W^{o}], is not shown in the reactive cycle for clarity. [Fe^{4+}=O W^{o}]$_W$ stands for the ferryl Trp-epoxide intermediate, when the Si site is occupied by Trp (as indicated by the subscripted “W”).

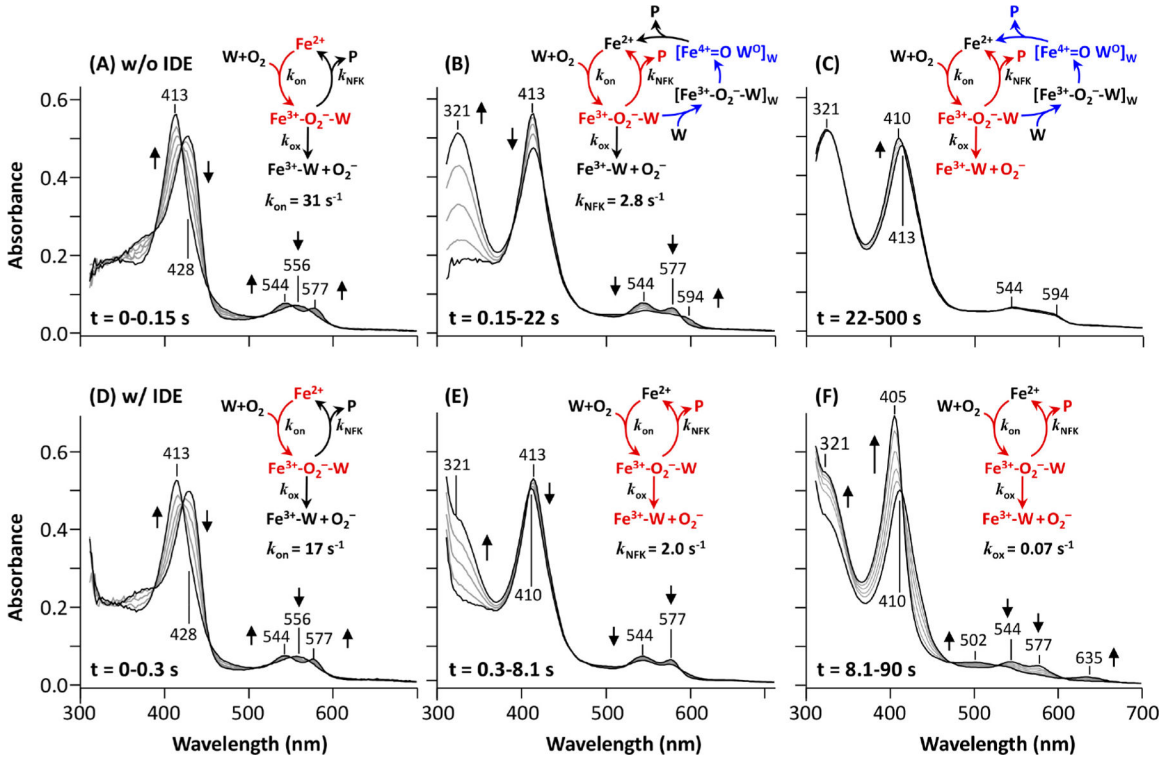

Figure 3.

Steady-state kinetics of hIDO1 in the absence (A–C) or presence (D–F) of IDE. The spectra were obtained as a function of time following the initiation of the reaction by mixing an air-saturated buffer with ferrous deoxy hIDO1 (in the presence of Trp) in the absence or presence of IDE in a stopped-flow system at 10 °C. The final [hIDO1], [O_2], [Trp], and [IDE] were 4 μM, 125 μM, 150 μM, and 2 mM, respectively, after mixing. The time window associated with the spectral data shown in each panel is indicated in the lower left corner. It is noted that the time window in (C) is >5 times larger than that in (F). A schematic illustration of the reaction cycle is shown in the inset in each panel, where the elementary steps of the reaction occurring within the given time window, as well as the detectable intermediates, are highlighted in red and blue. The notations are defined in Figure 2.

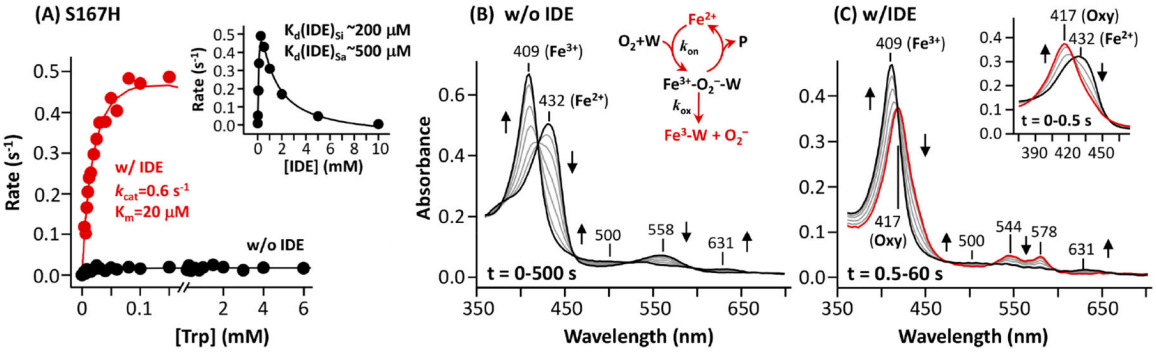

Figure 4.

Abolished activity of S167H and its rescue by IDE. (A) Turnover activity of S167H in the absence (black) or presence (red) of 100 μM IDE, obtained with 0.25 μM enzyme. The inset shows a plot of the enzyme activity as a function of [IDE], showing two distinct IDE binding sites. All the data were obtained at room temperature. (B–C) Stopped-flow data obtained by mixing an air-saturated buffer with deoxy S167H (in the presence of Trp) in the absence or presence of IDE at 20 °C. The final [hIDO1], [O_2], [Trp], and [IDE] were 4, 125, 100, and 100 μM, respectively, after mixing. The time window associated with the spectral data shown in each panel is indicated in the lower left corner. The inset in (C) shows the spectra obtained during the initial stage of the reaction (0–0.5 s). “Oxy” stands for the active ternary complex.

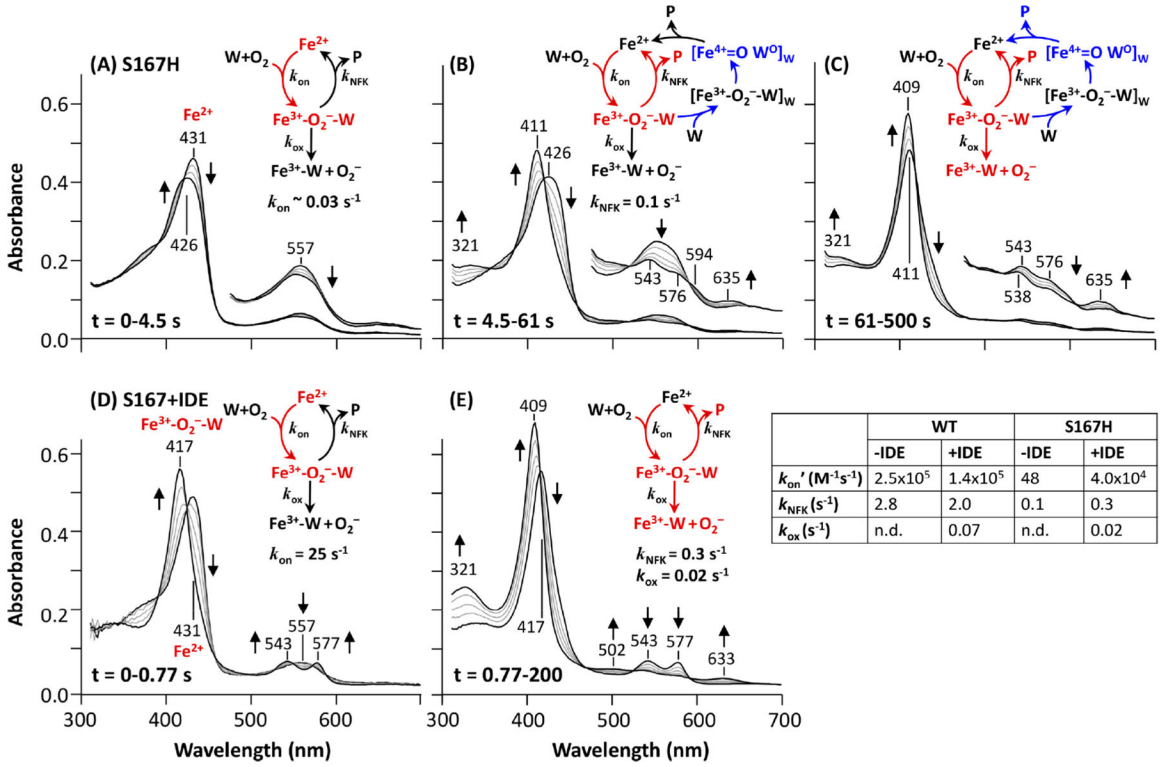

	WT		S167H	
	-IDE	+IDE	-IDE	+IDE
k_{on}' ($M^{-1}s^{-1}$)	2.5x10^5	1.4x10^5	48	4.0x10^4
k_{NFK} (s^{-1})	2.8	2.0	0.1	0.3
k_{ox} (s^{-1})	n.d.	0.07	n.d.	0.02

Figure 5.

Steady-state kinetics of S167H in the absence (A–C) or presence (D–E) of IDE. The spectra were obtained as a function of time following the initiation of the reaction by mixing an O_2-saturated buffer with ferrous deoxy S167H (in the presence of Trp) in the absence or presence of IDE in a stopped-flow system at 10 °C. The final [hIDO1], [O_2], [Trp], and [IDE] were 4, 625, 100, and 100 μM, respectively, after mixing. The time window associated with the spectral data shown in each panel is indicated in the lower left corner. It is noted that the time window in (C) is >2 times larger than that in (E). A schematic illustration of the reaction cycle is shown in the inset in each panel, where the elementary steps of the reaction occurring within the given time window, as well as the detectable intermediates, are highlighted in red and blue. The notations are defined in Figure 2. The right inset in (E) summarizes the key kinetic constants associated with the wild-type (WT) and the S167H reactions, where k_{on}' stands for the bimolecular O_2 binding rate constant calculated from the observed k_{on} based on the [O_2] employed for each reaction.

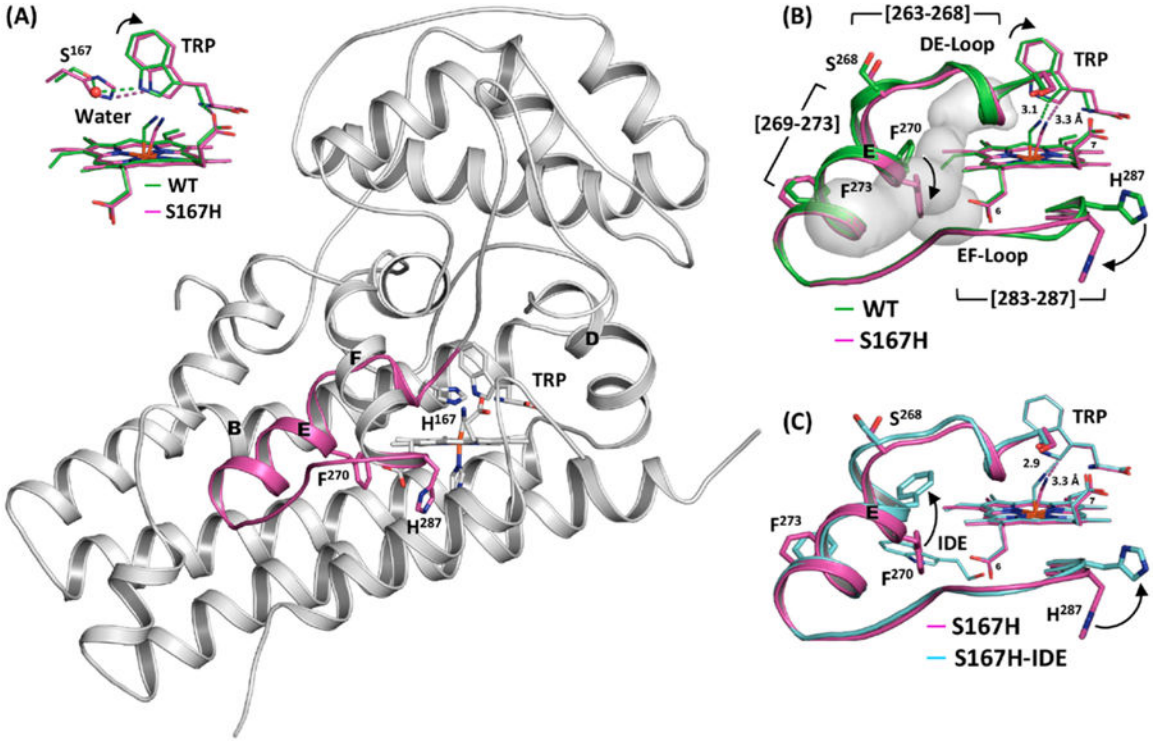

Figure 6.

Crystal structure of the S167H mutant of hIDO1. (A) Overall structure of the S167H mutant. The major structural perturbation introduced by the mutation is highlighted in magenta. The substrate Trp, heme, and the heme ligands (CN and H346) are shown as gray sticks. The upper left inset highlights the direct H-bond between H167 and the indoleamine in the S167H mutant versus the water-mediated H-bonds between S167 and the indoleamine group of the substrate Trp in the wild-type enzyme. (B) Expanded view of the major structural change induced by S167H mutation, where the structures of the S167H-CN-Trp complex and the wild-type complex (PDB code: 5WMU) are shown in magenta and green, respectively. The hypothesize ligand delivery tunnel is shown in gray surface representation. (C) Structural change introduced by IDE binding to the Si site in the S167H mutant. The structures of the S167H-CN-Trp complexes without and with IDE are shown in magenta and cyan, respectively.

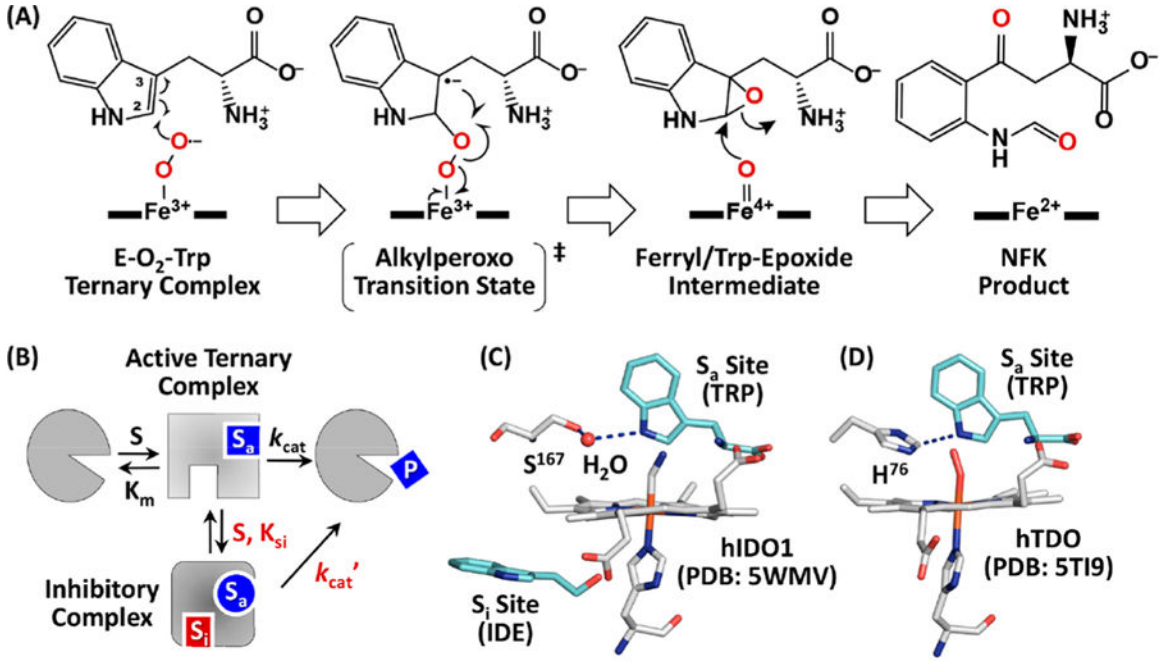

Scheme 1.

Two-Step Ferryl-Based Dioxygenase Mechanism of hIDO1 and hTDO (A), Two-Trp Binding Sites Model Accounting for the Substrate-Inhibition Behavior of hIDO1 (B), Active Site Structure of the hIDO1-CN-Trp Complex with the Si Site Occupied by IDE (C), and Active Site Structure of the hTDO-O_2-Trp Complex (D)